VT-NMR Analysis of Rotation-Inversion of *N*-(4-hydroxybutyl)-*N*-(2,2,2-trifluoroethyl) *tert*-butyl carbamate: Utilizing the $-CH_2CF_3$ Appendage as a Reporter on *E*/*Z*-Isomerization

Brian Jameson[a] and Rainer Glaser*,[a]

[a] Dr. Brian Jameson, Prof. Dr. Rainer Glaser*

Department of Chemistry, Missouri University of Science and Technology, Rolla, Missouri 65409, United States.

Email: glaserr@umsystem.edu

Graphical Abstract

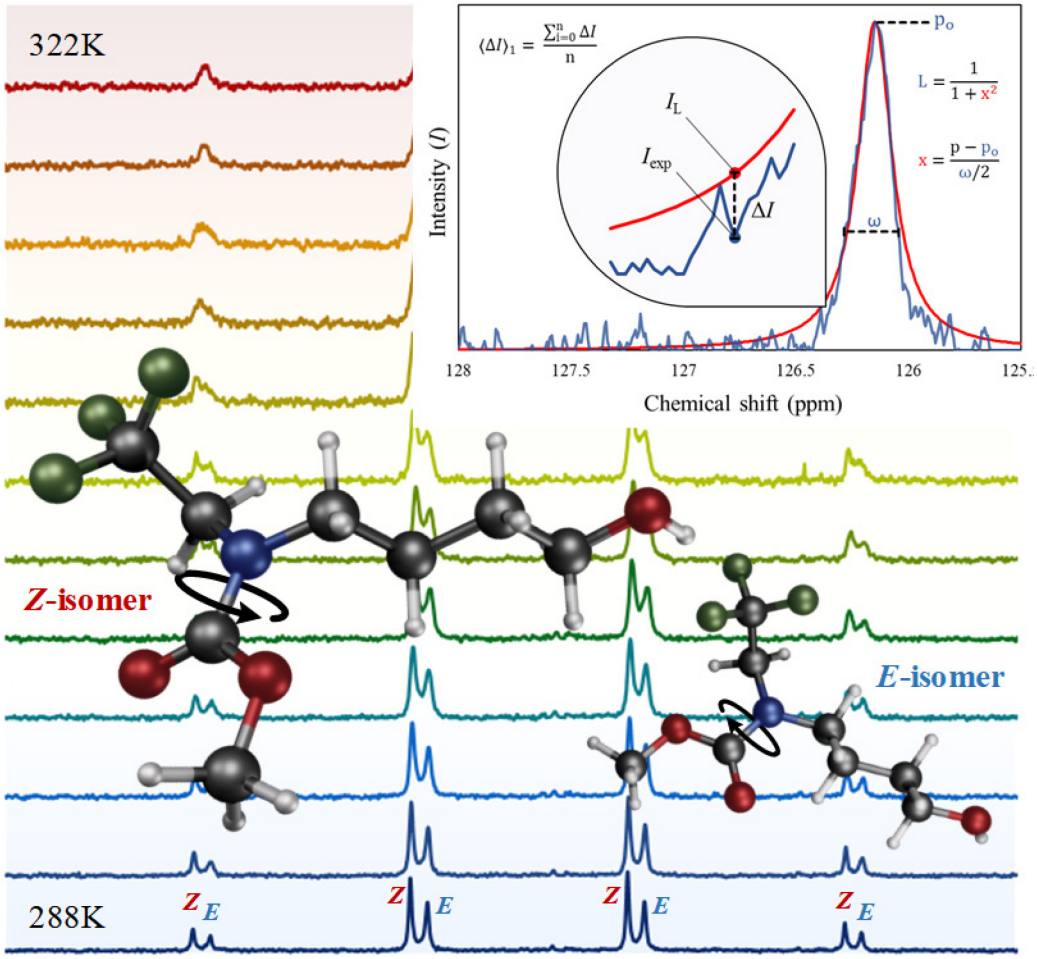

J(¹³C,¹⁹F) Coupled ¹³CNMR Spectra

ToC Text

The CF_3 group in the $-CH_2CF_3$ appendage reports on *E*/*Z*-isomerization in carbamates. The CN rotational barrier of *N*-(4-hydroxybutyl)-*N*-(2,2,2-trifluoroethyl) *tert*-butyl carbamate was quantified with Eyring-Polanyi theory via variable temperature ^{13}C and ^{19}F NMR spectroscopy in conjunction with innovative Lorentzian line shape analysis informed by data covering the entire temperature range.

Abstract

The rotational barrier about the CN carbamate bond of *N*-(4-hydroxybutyl)-*N*-(2,2,2-trifluoroethyl) *tert*-butyl carbamate **1** was determined by variable temperature (VT) ^{13}C and ^{19}F NMR spectroscopy. The $-CH_2CF_3$ appendage reports on rotational isomerism and allows for the observation of separate signals for the *E*- and *Z*-ensembles at low temperature. The activation barrier for *E*/*Z*-isomerization was quantified using Eyring-Polanyi theory which requires the measurements of the maximum difference in Larmor frequency $\Delta\nu_{max}$ and the convergence temperature T_c. Both $\Delta\nu_{max}$ and T_c were interpolated by analyzing sigmoidal functions fitted to data describing signal separation and the quality of the superposition of the *E*- and *Z*-signals, respectively. Methods for generating the quality-of-fit parameters for Lorentzian line shape analysis are discussed. Our best experimental value for the rotational barrier $\Delta G_c^{\ddagger}$(**1**) = 15.65±0.13 kcal/mol is compared to results of a higher level ab initio study of the model *N*-ethyl-*N*-(2,2,2-trifluoroethyl) methyl carbamate.

Introduction

The rotational barrier of CN bonds in amides $R_1R_2N{-}CO{-}R_3$ has been the subject of detailed study because of their relevance to peptide chemistry and it is a prime example in any discussion of resonance theory. Defining characteristics include *N*-sp^2 geometry of their *E*- and *Z*-minima, and *N*-sp^3 geometry of their pyramidal transition state (TS) structures.[1-4] Ureas $R_1R_2N{-}CO{-}NR_3R_4$ and carbamates $R_1R_2N{-}CO{-}OR_3$ show similar *E*/*Z*-isomerism and TS-pyramidalization. The hindered rotation of ureas has been subject of several investigations including the work on urea itself by Stilbs and Forsén[5] and the quantification of the barriers of a series of alkyl substituted ureas by Bryantsev et al.[6] Carbamates exhibit similar *E*/*Z*-conformational isomerism[7-10] but much less is known about their rotational dynamics.

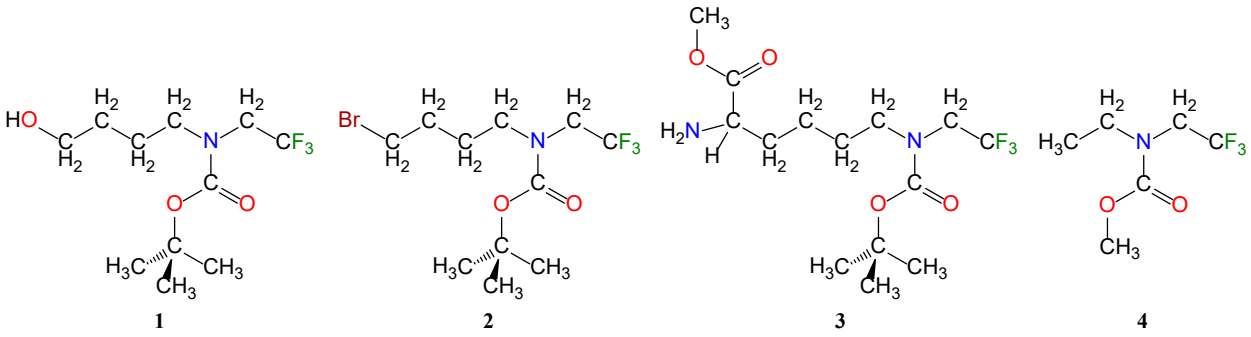

Scheme 1. Carbamate intermediates in the synthesis of N^{ε}-(2,2,2-trifluoroethyl)-*L*-lysine **1**-**3** and model compound **4**.

While developing a synthetic route for generating *N*-trifluoroethyl functionalized lysine and analogs, we observed two ^{13}C NMR quartet signals corresponding to a single CF_3 carbon for *tert*-butyloxycarbonyl (BOC) protected intermediates including *N*-(4-hydroxybutyl)-*N*-(2,2,2-trifluoroethyl) *tert*-butyl carbamate **1**, *N*-Boc-*N*-(2,2,2-trifluoroethyl)-4-bromobutan-1-amine **2**, N^{ε}-Boc-N^{ε}-(2,2,2-trifluoroethyl)-*L*-lysinate **3** (Scheme 1).[11] Analysis of the potential energy surface (PES) of the model system *N*-ethyl-*N*-(2,2,2-trifluoroethyl) methyl carbamate **4** showed a

large barrier to rotation-inversion about the CN bond.[12] The presence of two *E*/*Z*-ensembles and of *eight* unique pathways connecting the minima created a complicated multi-paths scenario and the application of proper Boltzmann statistics was required to model the experimentally measured rotational barrier.

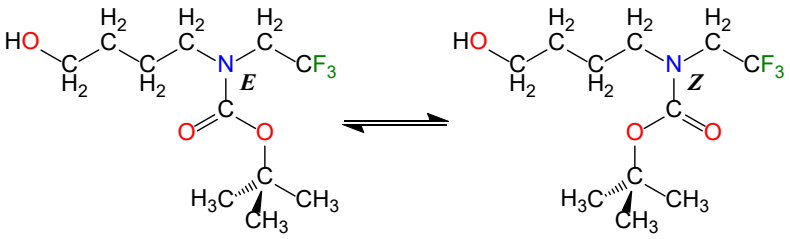

Scheme 2. The *E*-**1** (left) and *Z*-**1** (right) rotational isomers of *N*-(4-hydroxybutyl)-*N*-(2,2,2-trifluoroethyl) *tert*-butyl carbamate.

To inform our computational work and to create a direct connection to experimentation, we measured the rotation-inversion barrier of **1**, the carbamate most similar to the computed model system **4**. Here we report on the experimental determination of the CN rotation-inversion barrier of *E*-**1** ⇌ *Z*-**1** (Scheme 2) by variable temperature (VT) NMR spectroscopy and its evaluation of the Eyring-Polanyi equation (Eq. 1) for the rate of rotamer exchange k_r as a function of the activation energy $\Delta G^{\ddagger}$ and of temperature T.[13.14] The preexponential factor

$$k_r = \frac{\kappa k_B T}{h} e^{-\frac{\Delta G^{\ddagger}}{RT}} \quad \text{(Eq. 1)}$$

$$\Delta G_c^{\ddagger} = 19.14 T_c \left[10.32 + \log\left(\frac{T_c}{k_c}\right)\right] \text{ J/mol} \quad \text{(Eq. 2)}$$

$$k_c = \frac{\pi \Delta \nu_{max}}{\sqrt{2}} \quad \text{(Eq. 3)}$$

includes the transmission coefficient κ, Boltzmann's constant k_B, and Planck's constant h.[15-17] The transmission coefficient κ is a measure of the fraction of transition state structures that effect product formation and is assumed to be $\kappa \approx 1$ for bond rotations. The rotational barrier is the minimum energy at which bond rotation becomes possible and its value can be determined by measuring the coalescence temperature T_c and the rate constant for rotamer exchange k_c via VT NMR spectroscopy (Eqs. 2 and 3).[18] The rate constant k_r depends only on the difference in chemical shift of the two rotamer signals $\Delta\nu$ (Hz), and at the coalescence temperature, k_c is a function of the *maximum* difference in chemical shift of the two rotamer signals $\Delta\nu_{max}$.

Several automated systems are available for the determination of T_c via the generation of line shapes of a given chemical environment by generating a list of transitions and their probabilities which can then be used to produce a computational estimate of the FID.[19] These programs are successful at simulating chemical exchange data from spectra of numerous compounds including 10-membered ring compounds containing amide and disulfide functionality.[20] We thought it important to determine this value explicitly via a quality of fit parameter which we derive as a function temperature to ensure the most accurate line-fit to our data (*vide infra*). Two strategies were employed to improve the accuracy and reliability of the measured rotational barrier. First, several data fitting and Lorentzian line shape analysis methods were developed to increase the accuracy of T_c and $\Delta\nu_{max}$ (*vide infra*). Second, the Eyring-Polanyi equation was evaluated by analyzing the *T*-dependent coalescence using both ^{13}C and ^{19}F NMR spectroscopy. ^{19}F NMR spectroscopy has been applied very successfully for medical MRI imaging using small fluorinated probes[21] as well as polymers containing the *N*-(2,2,2-trifluoroethyl) appendage,[22] to distinguish binding sites in large proteins via biomolecular ^{19}F-labeling,[23] and for cell labeling with *N*-(2,2,2-trifluoroethyl) cyclam derivatives.[24] We will show that ^{19}F NMR spectroscopy is superior to ^{13}C NMR for coalescence studies of *E*/*Z*-isomerization and that the presence of the CH_2CF_3 appendage amplifies the advantage.

Experimental Methods

N-(4-hydroxybutyl)-*N*-(2,2,2-trifluoroethyl) *tert*-butyl carbamate **1** was synthesized by reductive amination of 4-amino-1-butanol with trifluoroacetaldehyde ethyl hemiacetal followed by Boc protection.[11] Deuterated chloroform $CDCl_3$ was procured from Sigma-Aldrich. NMR spectra were acquired using a Bruker 400 MHz Avance III HD liquid state NMR spectrometer. Two Bruker pulse programs were employed in this study: the ^{1}H-decoupled ^{13}C pulse program *zgpg30*, and the ^{1}H-decoupled ^{19}F pulse program *zgfhigqn.2* each preformed with scan counts of $s(^{13}C) = 1000$ and $s(^{19}F) = 64$, respectively.

Results and Discussion

^{13}C and ^{19}F NMR Spectra of the CF_3 group of 1 as Function of Temperature

^{13}C and ^{19}F NMR spectra were acquired for **1** over a temperature range of 288 - 322 K **(**Figure 1). While the ^{1}H NMR spectra did not give adequate resolution of the $-C\mathbf{H_2}CF_3$ quartet signals of the *E*- and *Z*-ensembles, both the ^{13}C and ^{19}F NMR spectra showed clear resolution of the $-CH_2\mathbf{CF_3}$ group and both featured larger *E*/*Z*-isomer splitting. In the ^{13}C NMR spectra (Figure 1, left), the CF_3 signal of each rotamer ensemble appears as quartet due to $^{1}J(^{13}C,^{19}F)$ coupling to three neighboring fluorines. In the ^{19}F NMR spectra (Figure 1, right), the CF_3 signals of the rotamers appear as singlets due to $^{3}J(^{19}F,^{1}H)$ decoupling.

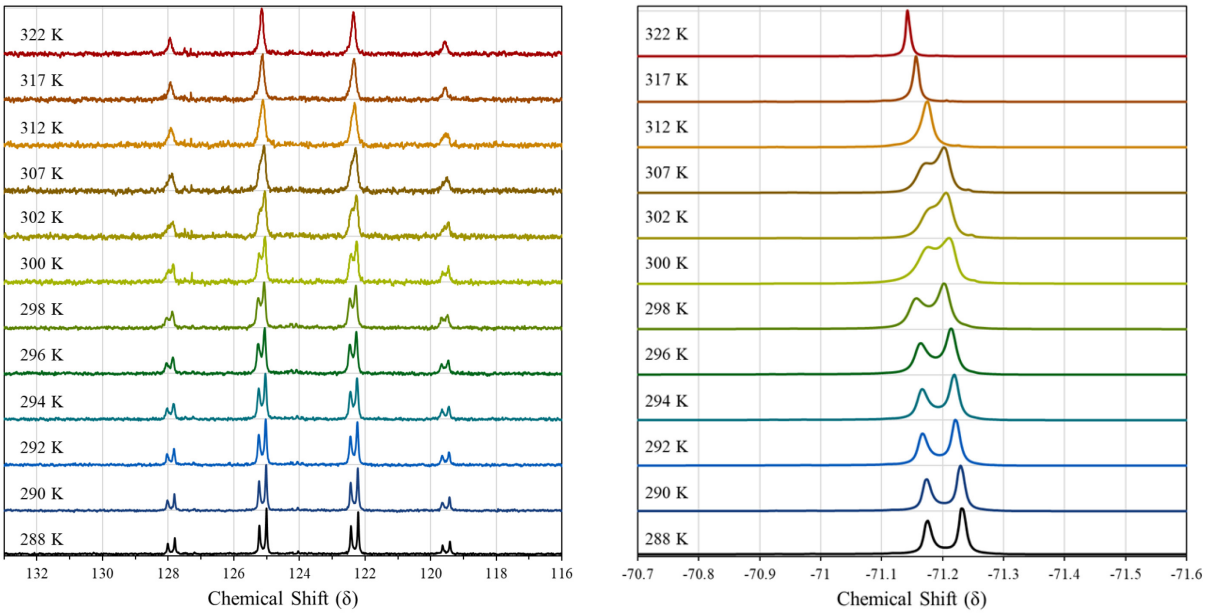

Figure 1. ^{13}C NMR spectra (left) and ^{19}F NMR spectra (right) of the CF_3 group of *N*-(4-hydroxybutyl)-*N*-(2,2,2-trifluoroethyl) *tert*-butyl carbamate **1** as a function of temperature.

Table 1. ^{13}C and ^{19}F NMR Data of the CF_3 group for *N*-(4-hydroxybutyl)-*N*-(2,2,2-trifluoroethyl) *tert*-butyl carbamate **1**[a-d]

Temperature	**$\delta(^{13}C)$** [ppm]		**$\Delta\nu(^{13}C)$**	**$\delta(^{19}F)$** [ppm]		**$\Delta\nu(^{19}F)$**	**$^1J(^{13}C,^{19}F)$** [Hz]		**$\Delta J(^{13}C, ^{19}F)$**
[*K*]	*E*-Rotamer	*Z*-Rotamer	[Hz]	*E*-Rotamer	*Z*-Rotamer	[Hz]	*E*-Rotamer	*Z*-Rotamer	[Hz]
289	124.83	123.61	87.80	-71.18	-71.23	22.52	283.26	282.63	0.63
290	124.83	123.61	87.80	-71.17	-71.23	22.20	283.22	282.57	0.65
291	124.84	123.62	85.60	-71.17	-71.22	21.92	283.24	282.60	0.64
292	124.80	123.58	86.60	-71.17	-71.22	21.68	283.18	282.51	0.67
293	124.84	123.63	83.60	-71.16	-71.22	21.12	283.25	282.63	0.62
294	124.80	123.59	84.36	-71.17	-71.22	21.04	283.17	282.54	0.63
295	124.85	123.65	80.62	-71.16	-71.21	20.24	283.26	282.66	0.60
296	124.80	123.59	81.42	-71.16	-71.21	19.76	283.15	282.54	0.61
297	124.86	123.66	79.56	-71.16	-71.21	19.68	283.30	282.70	0.60
298	124.81	123.62	79.62	-71.16	-71.20	17.68	283.19	282.59	0.60
299	124.86	123.69	70.86	-71.15	-71.20	16.72	283.30	282.76	0.54
300	124.86	123.69	71.26	-70.95	-70.99	14.52	283.30	282.75	0.55
301	124.83	123.66	68.20	-70.92	-70.95	13.60	283.22	282.68	0.54
302	124.81	123.66	59.80	-70.91	-70.94	9.16	283.19	282.70	0.49
303	124.78	123.66	50.00	-70.90	-70.92	5.20	283.12	282.69	0.43
304	124.81	123.69	47.40	-70.90	-70.91	2.00	283.17	282.76	0.41
305	124.77	123.69	32.40	~	~	~	283.09	282.76	0.33
306	123.77	123.71	22.00	~	~	~	283.08	282.79	0.29
307	124.76	123.72	18.40	~	~	~	283.07	282.82	0.25
308	124.77	123.73	12.60	~	~	~	283.08	282.86	0.22
309	124.75	123.73	6.60	~	~	~	283.04	282.86	0.18
310	123.76	123.74	6.00	~	~	~	283.05	282.88	0.17

[a] Chemical shift and *J*-coupling constants for $T > 304$ K for the ^{19}F NMR data and $T > 310$ K for the ^{13}C NMR data are not discernable. [b] The $\delta(^{13}C)$ values specify the position of center of the quartet as measured by the two larger inner peaks. [c] See text for rotamer assignment (*vide infra*). [d] The reported difference in chemical shifts $\Delta\nu$ at high temperatures is an apparent difference in chemical shift due to convolution of the overlapping signals.

The experimental chemical shifts $\delta(^{13}C)$ and $\delta(^{19}F)$ and the $^{1}J(^{13}C,^{19}F)$ coupling constants for **1** are shown as a function of temperature (Table 1) for the two rotamers along with the differences $\Delta\nu(^{13}C)$, $\Delta\nu(^{19}F)$, and $\Delta^{1}J(^{13}C,^{19}F)$. The reported $J(^{13}C,^{19}F)$ coupled $\delta(^{13}C)$ chemical shifts refer to the centers of the quartet signals of the *E*- and *Z*- rotamer signals. The differences in Larmor frequencies $\Delta\nu(^{13}C)$ and $\Delta\nu(^{19}F)$ of the two rotamer signals decrease with increasing temperature; however, the ^{19}F singlets coalesce at a lower temperature than the ^{13}C quartets. As such the ^{19}F chemical shift data is only reported up to 304 K. The reported difference in chemical shifts $\Delta\nu$ at high temperatures is an apparent difference in chemical shift due to convolution of the overlapping signals.

Population Analysis of the *E*- and *Z*- Ensembles of Carbamates 1 and 4

In Scheme 3 are shown two sets of *E*/*Z* rotamers of **1** in analogy to the results of the structural study of **4**. Model system **4** features the same carbamate and fluorine functionality as **1** and two sets of *E*/*Z* rotamers were found by optimization of structures of **4** at the MP2/6-311++G(d,p) level.[12] The minima of each rotamer ensemble are defined by the orientation of the carbamate (*E* or *Z*) and by the orientation of the *N*-alkyl substituents. The *N*-alkyl substituents may be on opposite faces of the carbamate plane (**a** structures) or on the same face (**b** structures). Computational determination of the NMR properties of the minima of **4** revealed that the *E*-rotamers had a higher chemical shift than the *Z*-rotamers. We assign the two CF_3 signals of **1** in analogy to **4**, and we will show that this assignment is fully consistent with the NMR measurements of **1**.

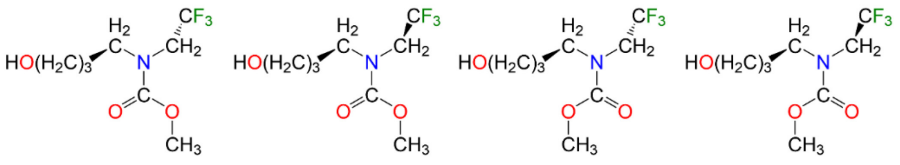

Scheme 3. The *E*- and *Z*-ensembles of **1**.

Integration of the ^{13}C and ^{19}F rotamer signals at our lowest temperature gave direct insight into each ensemble's population (Figure 2). The integrations of the higher frequency signals of ensemble [*E*-**1**] = {*E*-**1a**, *E*-**1b**} and of the lower frequency signals of ensemble [*Z*-**1**] = {*Z*-**1a**, *Z*-**1b**} allow for the determination of the populations of each ensemble; p(*E*-**1**) = [*E*-**1**] / ([*E*-**1**] + [*Z*-**1**]) and p(*Z*-**1**) = [*Z*-**1**] / ([*E*-**1**] + [*Z*-**1**]). At 288 K the tail-ends of each rotamer signal show partial overlap and lowering the temperature does not split the *E*/*Z*-signals further. The populations were determined to be p(*E*-**1**) ≈ 45% and p(*Z*-**1**) ≈ 55%. The rotamer populations p(*E*-**4**) = 44% and p(*Z*-**4**) = 56% were determined[12] using the energies of the *E*/*Z*-minima of **4** computed at the MP4/6-311++G(d,p)//MP2/6-311++G(d,p) level, and their good agreement with the measured populations of **1** justifies the selection of **4** as a suitable model system.

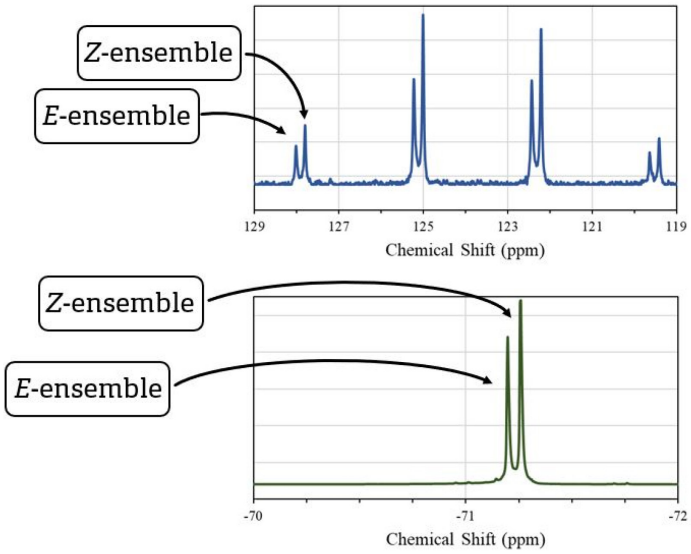

Figure 2. The signals associated with the *E*/*Z*-ensembles in the ^{13}C (top, blue) and ^{19}F (bottom, green) NMR spectra of **1** at 289 K.

$\Delta^1J(^{13}C,^{19}F)$ as a Function of Temperature

VT NMR spectroscopy of the *E*/*Z* ensembles allows for the measurement of $^1J(^{13}C,^{19}F)$ coupling constants of each rotamer as function of temperature (Table 1). Studies related to *T*-

dependence of *J*-coupling constants of rotamers are rare and an interesting case was investigated by Reynolds and Wood in their study of the *T*-dependence on the vicinal *J*-coupling constants of conformations of (1,2-dibromoethyl)benzene.[25] Figure 3 shows that the magnitude of the $^{1}J(^{13}C,^{19}F)$ coupling constant of the high frequency signal (*E*-ensemble, blue) decreases with increasing temperature, whereas the magnitude for the low frequency signal (*Z*-ensemble, red) increases. Consequently, the difference $\Delta^{1}J(^{13}C,^{19}F)$ decreases with increasing temperature until the observed $^{1}J(^{13}C,^{19}F)$ coupling constant approaches $^{1}J(^{13}C,^{19}F)_{323K}$ = 282.97 Hz (Figure 3, yellow line). This measured value closely agrees with the Boltzmann average of the two ensembles $^{1}J(^{13}C,^{19}F)_{289K}$ = 282.91 Hz (Figure 3, green dotted line) calculated with the $^{1}J(^{13}C,^{19}F)$ coupling constants and populations of each ensemble at 289 K.

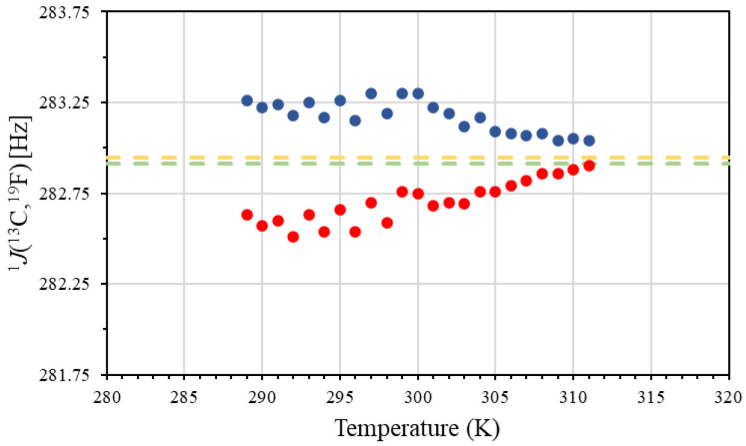

Figure 3. The $^{1}J(^{13}C,^{19}F)$ coupling constant of the *E*-ensemble (blue) and *Z*-ensemble (red) plotted as a function of temperature, the observed $^{1}J(^{13}C,^{19}F)_{323K}$ coupling constant (yellow), and the Boltzmann averaged $^{1}J(^{13}C,^{19}F)_{289K}$ coupling constant (green).

Difference in Larmor Frequencies Δν of the *E*- and *Z*-Ensembles

The differences in the Larmor frequencies of the two rotamers Δν (Hz) were plotted as a function of temperature for the ^{13}C (left) and ^{19}F (right) NMR spectra (Figure 4). Sigmoidal line fits $\sigma_C(T)$ and $\sigma_F(T)$ (primary y-axis) are shown in Figure 3 and they are defined by Eq. 4. Constants A-D in Eq. 4 were determined by iterative nonlinear regression minimization of an error function using the *solver* add-on in excel.[26]

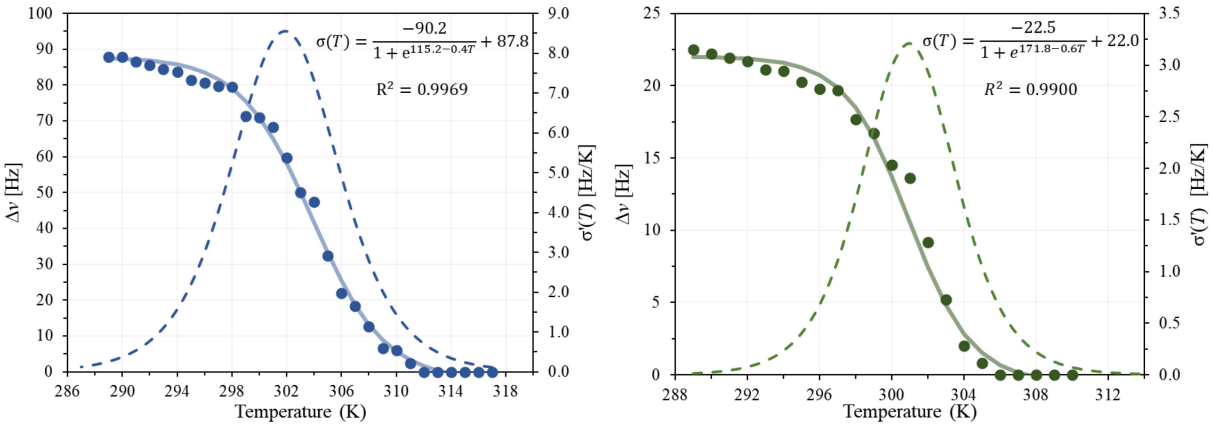

Figure 4. Difference in the rotamer Larmor frequencies of the CF_3 group of **1** are plotted as a function of temperature Δν(^{13}C) (left, blue) and Δν(^{19}F) (right, green) along with the sigmoidal line fits σ(T) (solid curves) and their gradients σ′(T) (dashed curves).

$$\sigma(T) = \frac{A}{1+e^{-BT+C}} + D \qquad \text{(Eq. 4)}$$

$$\sigma'(T) = \frac{-AB(e^{-BT+C})}{(1+e^{-BT+C})^2} \qquad \text{(Eq. 5)}$$

$$\Delta\nu_{max} = \lim_{T\to 0} \sigma(T) \qquad \text{(Eq. 6)}$$

The gradient σ′(T) (Eq. 5) describes the rate of convergence of the rotamer signals (secondary y-axis) and it is the first derivative of the sigmoidal line fit. The greatest convergence of the two ensembles occurs at T = 303.9 K with $\sigma'(T)_{max}$ = 8.6 Hz/K for the ^{13}C NMR spectra and at T = 300.9 K with $\sigma'(T)_{max}$ = 3.2 Hz/K for the ^{19}F NMR spectra, respectively.

The maximum difference in the Larmor frequencies of the rotamers $\Delta\nu_{max}$ was determined by extrapolation of the sigmoidal line fit to the limit $T \rightarrow 0$ K (Eq. 6). For the ^{13}C and ^{19}F NMR data, these extrapolations yielded the values $\Delta\nu_{max}(^{13}C) = 87.80\pm2.09$ Hz and $\Delta\nu_{max}(^{19}F) = 22.00\pm2.30$ Hz. The difference in $\Delta\nu_{max}$ between the ^{13}C and ^{19}F data sets is $\Delta\Delta\nu_{max}(\mathbf{1}) = 65.8\pm3.11$ Hz.

The chemical shifts of the carbon and of the three fluorine nuclei in the CF_3 appendage of model **4** were calculated at the BHandHLYP/6-311++G(3df,3pd) level at 289 K and the numbers computed at this level are representative of the performance of several computational levels.[12] The differences between the rotamer signals for **4** were determined to be $\Delta\nu_{max}(^{13}C) = 123.86$ Hz and $\Delta\nu_{max}(^{19}F) = 60.87$ Hz. We note that the chemical shift of one fluorine proximate to the carbamate group is significantly lower (~6.42 ppm) compared to the other two, and $\Delta\nu_{max}(^{19}F)$ is the average and assumes fast rotation about the C-CF_3 bond. Although the computed values of $\Delta\nu_{max}(^{13}C)$ and $\Delta\nu_{max}(^{19}F)$ for **4** do not agree well with the absolute values measured for **1**, $\Delta\Delta\nu_{max}(\mathbf{4}) = 63.0$ Hz closely agrees with $\Delta\Delta\nu_{max}(\mathbf{1}) = 65.8\pm3.11$ Hz.

Coalescence Temperature T_c via Lorentzian Line Shape Analysis

It is fairly easy to decide by visual inspection of spectra whether two peaks remain separate at a given temperature. It is much harder to decide at which temperature complete coalescence has occurred. At temperatures where merging peaks are clearly no longer separated, line shape analysis allows for the decision between superposition of closely positioned overlapping peaks and true coalescence. Only in the latter case will the observed peak be well described by a Lorentzian function; that is to say, the deviation of a measured peak from the Lorentzian line shape informs as to whether complete coalescence has been achieved. There will always be a residual deviation between the measured line shape and an ideal Lorentzian line shape because of inherent experimental error. Assuming that the deviation due to experimental

error is a constant for a given device, coalescence is complete if the first derivative of the quality-of-fit function approaches zero.

The two CF_3 rotamer signals of **1** converge with increasing temperature to one quartet in the ^{13}C NMR spectra and one singlet in the ^{19}F NMR spectra. Spectra acquired above 310 K and 304 K for the ^{13}C and ^{19}F NMR data sets were nearly indistinguishable, making a quantitative determination of the true coalescence temperature T_c difficult. Line shape analysis was employed over a temperature range of 288-323 K for both nuclei via Lorentzian line fitting (Eq. 7 and Eq. 8). The Lorentzian function L is a function of the maximum intensity I_o and the variable x which is defined by a chemical shift p, the chemical shift at maximum intensity p_o, and the full spectral width at half maximum intensity ω.[27]

$$L = \frac{I_o}{1+x^2} \qquad \text{(Eq. 7)}$$

$$x = \frac{p-p_o}{\omega/2} \qquad \text{(Eq. 8)}$$

The fit of a Lorentzian function to the experimentally measured discrete data points in the signal region is quantified by the absolute intensity differences $\Delta I = |I_L - I_{exp}|$ between the Lorentzian function intensities I_L and the experimental intensities I_{exp}. Figure 5 illustrates the Lorentzian line shape analysis for one of the inner quartet peaks of the ^{13}C NMR spectrum at 312 K. Figure 5 shows the experimental data points I_{exp} in blue and the Lorentzian I_L values computed for the same chemical shifts in red. The ΔI values were determined for a relatively narrow chemical shift range ($p_o \pm 0.5$ ppm) to reduce background noise, and averaging over n = 279 chemical shift pairs resulted in $\langle \Delta I \rangle_1$ via Eq. 9 for a single quartet peak. In analogy, the quality of an analysis of two peaks can be assessed via $\langle \Delta I \rangle_2$ (Eq. 10), and we performed a joint analysis of the two inner quartet peaks with n = 279 for each peak. The two outer quartet peaks were not included in the joint analysis due to their lower resolution. The high temperature ^{19}F NMR spectra of **1** only feature singlets and were evaluated via Eq. 9 with n = 272.

$$\langle \Delta I \rangle_1 = \frac{\sum_{i=1}^{n} \Delta I}{n} \qquad \text{(Eq. 9)}$$

$$\langle \Delta I \rangle_s = \sum_{j=1}^{s} \frac{\sum_{i=1}^{n} \Delta I}{n} \qquad \text{(Eq. 10)}$$

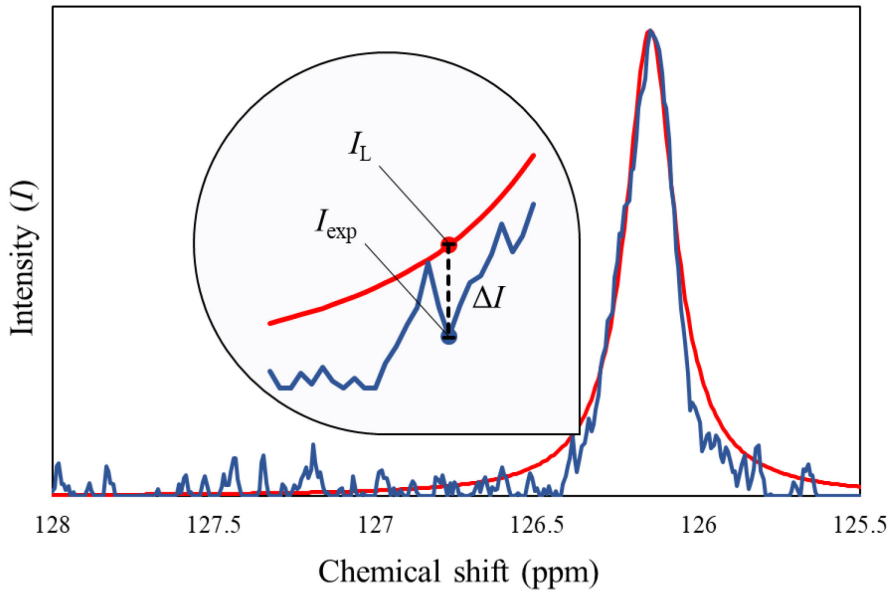

Figure 5. Determination of $\Delta I = |I_L\text{-}I_{exp}|$ values from the digitized experimental intensities I_{exp} (blue) and the Lorentzian function intensities I_L (red) determined at the same discrete chemical shifts.

The best way for the practical determination of the coalescence temperature T_c requires an analytical expression for the quality-of-fit parameter as a function of temperature $\langle \Delta I \rangle(T)$ and its derivative $\langle \Delta I \rangle'(T)$. With the derivative function known one can then determine T_c by way of selecting a threshold for the deviation of $\langle \Delta I \rangle'(T)$ from zero. For this approach to work the parameter $\langle \Delta I \rangle$ must be defined both at high *and* low temperatures. At high temperature one Lorentzian function closely describes one NMR signal as discussed above (Figure 5). However,

at low temperature one Lorentzian function serves as an average of the separated *E*- and *Z*-signals and this is illustrated in Figure 6.

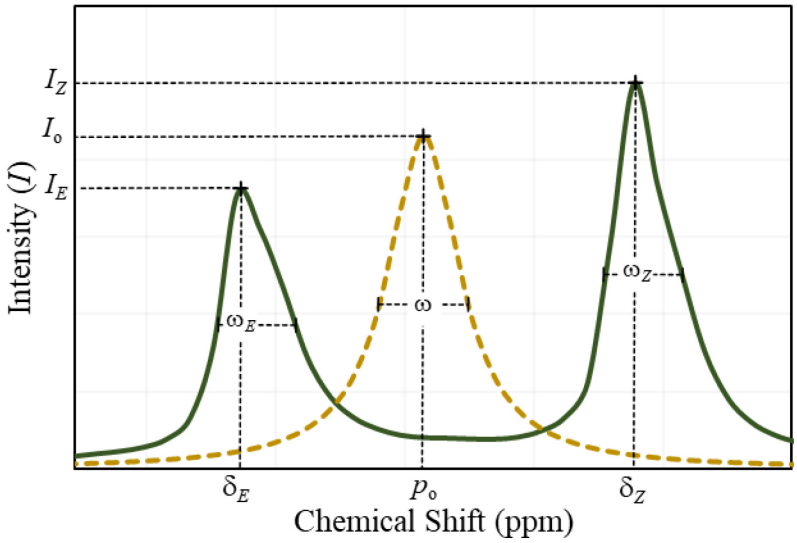

Figure 6. ^{19}F Spectrum at 288 K featuring the parameters necessary to build a Lorentzian line shape (yellow) from the *E*- and *Z*-signals (green).

The measured values p_o, I_o and ω at high temperatures describe the asymmetric signal of the merging peaks prior to perfect coalescence. At low temperature however, p_o, I_L and ω are functions of the separate *E*- and *Z*-signals as defined by Eqs. 11-13. The ^{13}C and ^{19}F spectra acquired below 310 K and 304 K, respectively, feature separated peaks for the *E*- and *Z*-isomers with spectral widths ω_E and ω_Z, and intensities I_E and I_Z. Low temperature spectra were fitted with Lorentzian functions (Figure 6) weighted according to the relative intensities and chemical shifts of the *E*- and *Z*-signals. Tables S1 and S2 list the chemical shifts at maximum intensity p_o, the maximum intensities I_L, and the full spectral widths at half maximum intensity ω for low temperature ^{13}C and ^{19}F spectra, respectively.

$$p_{\mathrm{o}} = \delta_Z + \frac{I_E}{I_E + I_Z} * |\delta_E - \delta_Z| \quad \text{(Eq. 11)}$$

$$I_{\mathrm{L}} = \frac{|p_{\mathrm{o}} - \delta_E|}{|\delta_E - \delta_Z|} * I_E + \frac{|p_{\mathrm{o}} - \delta_Z|}{|\delta_E - \delta_Z|} * I_Z \quad \text{(Eq. 12)}$$

$$\omega = \frac{|I_L - I_E|}{|I_E - I_Z|} * \omega_E + \frac{|I_L - I_Z|}{|I_E - I_Z|} * \omega_Z \quad \text{(Eq. 13)}$$

$$\langle \Delta I \rangle(T) = \frac{A}{1 + \mathrm{e}^{-BT+C}} + D \quad \text{(Eq. 14)}$$

$$\langle \Delta I \rangle'(T) = \frac{AB(\mathrm{e}^{-BT+C})}{(1 + \mathrm{e}^{-BT+C})^2} \quad \text{(Eq. 15)}$$

$$T_{\mathrm{c}} = \lim_{\langle \Delta I \rangle \to C} \langle \Delta I \rangle(T) = \lim_{\langle \Delta I \rangle \to 0} \langle \Delta I \rangle'(T) \quad \text{(Eq. 16)}$$

The averaged Lorentzian quality-of-fit parameters $\langle \Delta I \rangle$ were generated as a function of temperature and they are included in Tables S1 and S2. The parameter $\langle \Delta I \rangle$ is a constant at low temperatures for each data set where the *E*- and *Z*- ensembles no longer exchange, and the values are $\langle \Delta I \rangle_{13C} \approx 13.6$ and $\langle \Delta I \rangle_{19F} \approx 4.0$. At high temperature the parameter $\langle \Delta I \rangle$ approaches a small constant value, and they are $\langle \Delta I \rangle_{13C} \approx 1.3$ and $\langle \Delta I \rangle_{19F} \approx 0.4$. We found that a sigmoidal line fit $\langle \Delta I \rangle(T)$ describes the data well, and this function was applied to both data sets in Figure 7 to determine T_{c} (solid line, Eq. 14). The constants *A*-*D* in Eq. 14 were determined using the same nonlinear regression techniques employed in the sigmoidal line fitting of the $\Delta\nu$ data.[26] The gradient of the sigmoidal line fit $\langle \Delta I \rangle'(T)$ is the first derivative (dashed line, Eq. 15), and T_{c} was determined by extrapolation of the gradient $\langle \Delta I \rangle'(T)$ to the limit $\langle \Delta I \rangle \to 0$ (Eq. 16).

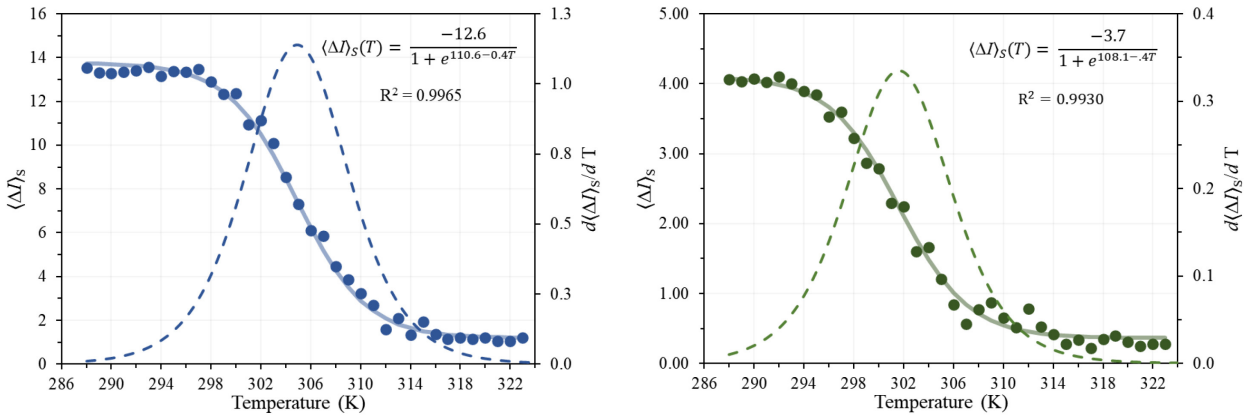

Figure 7. The quality-of-fit parameters $\langle\Delta I\rangle_S$ of **1** are plotted as a function of temperature for the ^{13}C data (blue, S = 2) and the ^{19}F data (green, S = 1). The sigmoidal line fit $\langle\Delta I\rangle(T)$ is applied to the combined data set and shown as a solid curve, and its gradient $\langle\Delta I\rangle'(T)$ is shown as a dotted curve.

As can be seen from Table 2, the choice of the threshold value of the gradient $\langle\Delta I\rangle'(T)$ significantly affects the corresponding coalescence temperature T_c. Evaluating Eq. 16 at very small values of $\langle\Delta I\rangle'(T)$ is not warranted considering the experimental error associated with $\langle\Delta I\rangle(T)$ and would suggest a high sensitivity of critical temperatures T_c to the choice of threshold (Figure 8). On the other hand, to choose a very large threshold of $\langle\Delta I\rangle'(T)$ would result in T_c values in the nonlinear region of the parent function $\langle\Delta I\rangle(T)$ (Figure 7). There is a sweet spot between these extremes and the assumption of a gradient threshold of $\langle\Delta I\rangle'(T) = 0.2$ affords the convergence temperatures $T_c(^{13}C) = 313.73$ K and $T_c(^{19}F) = 307.63$ K. In this region a change of the gradient threshold by $\Delta\langle\Delta I\rangle'(T) = \pm 0.1$ effects the determination of the critical temperature T_c by $\Delta T \approx 1.3$ K and we use this ΔT value as error bar to $T_c(^{13}C)$ and $T_c(^{19}F)$.

Table 2. $\langle \Delta I \rangle'(T)$ and $\Delta G_c^{\ddagger}$ as a Function of Temperature for the ^{13}C and ^{19}F Data Sets of **1**.

$\langle \Delta I \rangle'(T)$	$T_c(^{13}C)$	$\Delta G_c^{\ddagger}(^{13}C)$	±	$T_c(^{19}F)$	$\Delta G_c^{\ddagger}(^{19}F)$	±
0.005	323.67	15.61	0.11	317.25	16.16	0.13
0.010	321.75	15.51	0.11	315.30	16.05	0.13
0.020	319.83	15.41	0.11	313.45	15.95	0.13
0.030	318.70	15.36	0.11	312.35	15.90	0.13
0.050	317.26	15.28	0.11	311.00	15.83	0.13
0.100	315.53	15.20	0.11	309.25	15.73	0.13
0.150	314.47	15.14	0.12	308.28	15.68	0.13
0.200	313.73	15.11	0.12	307.63	15.65	0.13
0.250	313.17	15.08	0.12	307.15	15.62	0.13
0.300	312.72	15.06	0.12	306.77	15.60	0.13
0.350	312.34	15.04	0.12	306.46	15.59	0.13
0.400	312.02	15.02	0.12	306.21	15.57	0.13
0.450	311.75	15.01	0.12	305.99	15.56	0.13
0.500	311.50	15.00	0.12	305.80	15.55	0.13
0.550	311.29	14.98	0.12	305.63	15.54	0.13
0.600	311.09	14.97	0.12	305.48	15.53	0.13
0.650	310.91	14.97	0.12	305.35	15.53	0.13
0.700	310.75	14.96	0.12	305.23	15.52	0.13
0.750	310.60	14.95	0.12	305.12	15.52	0.13
0.800	310.46	14.94	0.12	305.03	15.51	0.13
0.850	310.34	14.94	0.12	304.93	15.51	0.13
0.900	310.22	14.93	0.12	304.85	15.50	0.13
0.950	310.11	14.93	0.12	304.77	15.50	0.13
1.000	310.00	14.92	0.12	304.70	15.49	0.13

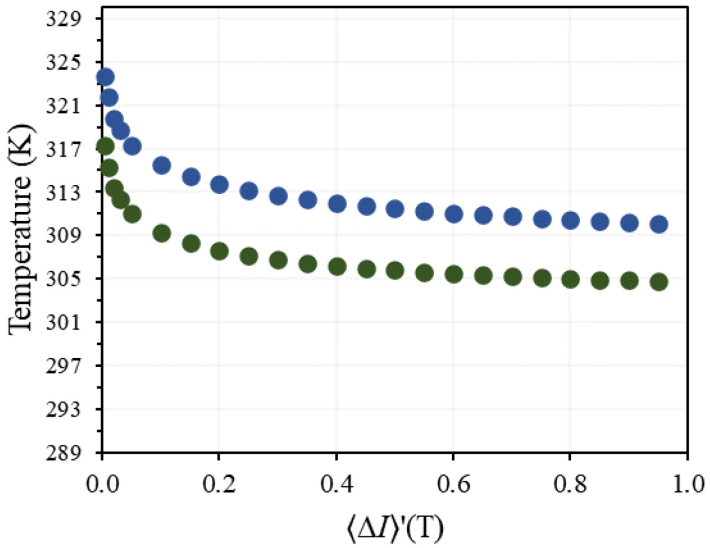

Figure 8. Change in temperature (K) with threshold values $\langle \Delta I \rangle'(T)$ of the ^{13}C data (blue) and the ^{19}F (green) data sets of **1**.

Rotational Barrier of Carbamate 1

Inserting the critical temperatures $T_c(^{13}C)$ = 313.73±1.4 K and $T_c(^{19}F)$ = 307.63±1.4 K, respectively, and the maximum differences in Larmor frequencies $\Delta\nu_{max}(^{13}C)$ = 87.80±2.09 Hz and $\Delta\nu_{max}(^{19}F)$ = 22.00±2.30 Hz, respectively, into the Eyring-Polanyi equation (Eq. 2) yielded the rotational barrier of **1** $\Delta G_c^{\ddagger}(^{13}C)$ = 15.11±0.12 kcal/mol and $\Delta G_c^{\ddagger}(^{19}F)$ = 15.65±0.13 kcal/mol. In Table 2 the error associated with the rotational barrier $\Delta G_c^{\ddagger}$ is listed as a "±" value immediately following the $\Delta G_c^{\ddagger}$ column, and this error was calculated with arithmetic error propagation of both T_c and $\Delta\nu_{max}$ in Eq. 2. Within the T_c±1.4 K range, Table 2 shows that the derived Gibbs' free energy of rotation falls in a narrow range of $\Delta(\Delta G_c^{\ddagger}) \approx 0.08$ kcal/mol which is lower than the $\Delta G_c^{\ddagger}$ propagated error.

The experimentally determined $\Delta G_c^{\ddagger}(^{13}C)$ and $\Delta G_c^{\ddagger}(^{19}F)$ values are not the same, they deviate by 3.5%, and their deviation exceeds the error bars computed based on the Lorentzian line shape analysis. The obvious questions are (a) which value best describes physical reality and (b) what causes this difference. The ^{19}F NMR spectra derived $\Delta G_c^{\ddagger}(^{19}F)$ value is far superior compared to the ^{13}C NMR spectra derived $\Delta G_c^{\ddagger}(^{13}C)$ value because the CF_3 group contains three ^{19}F atoms and one ^{13}C atom with natural abundances[28] of NA(^{19}F) = 99.99% and NA(^{13}C) = 1.07% and provides an intrinsic advantage for the ^{19}F NMR sensitivity by a factor of ~300. The carbon and fluorine spectra of **1** were recorded with scan counts of $s(^{13}C)$ = 1000 and $s(^{19}F)$ = 64. Because the signal-to-noise ratio (SNR) scales with the number of scans as SNR ~ $s^{0.5}$, the difference in the scan counts in the ^{13}C and ^{19}F NMR measurements only improves the carbon SNR by a factor of 4 relative to the fluorine SNR. It is simply not practical to increase the scan count $s(^{13}C)$ sufficiently to overcome the intrinsically different sensitivity of the nuclei.

Conclusion

The rotational barrier of *N*-(4-hydroxybutyl)-*N*-(2,2,2-trifluoroethyl) *tert*-butyl carbamate **1** was measured by variable temperature ^{13}C and ^{19}F NMR spectroscopy over a temperature range of 288-323 K. The determination of the rotational barrier requires the measurement of the maximum difference in chemical shift of the two rotamer signals $\Delta\nu_{max}$ and of the coalescence temperature T_c. While the determination of $\Delta\nu_{max}$ is relatively straightforward, the accurate determination of T_c requires sophisticated line shape analysis. The $\Delta\nu_{max}$ values were determined by analyzing the limit $T \rightarrow 0$ K of a sigmoidal function $\sigma(T)$ describing the discrete $\Delta\nu(T)$ values of the *E*- and *Z*-rotamers. The maximum differences in their Larmor frequencies were determined to be $\Delta\nu_{max}(^{13}C) = 87.80\pm2.09$ Hz and $\Delta\nu_{max}(^{19}F) = 22.00\pm2.30$ Hz.

We have shown that the determination of T_c by visual inspection alone is inadequate, and that Lorentzian line shape analysis is required to distinguish between closely positioned overlapping peaks and true coalescence. The fit of a Lorentzian function to an experimental data set was quantified via the absolute intensity difference $\Delta I = |I_L - I_{exp}|$ between the Lorentzian function intensities I_L and the experimental intensities I_{exp}. Coalescence is complete if the first derivative of the quality-of-fit function $\langle\Delta I\rangle(T)$ approaches zero. It is a significant outcome of our study that $\langle\Delta I\rangle(T)$ must me known both at high *and* low temperatures to ensure the proper fit of the data to the underlying sigmoidal function $\langle\Delta I\rangle(T)$.

The convergence temperature T_c was determined by evaluation of the gradient $\langle\Delta I\rangle'(T)$ to the limit $\langle\Delta I\rangle \rightarrow 0$. The choice of the threshold value of the gradient $\langle\Delta I\rangle'(T)$ significantly effects the corresponding coalescence temperature T_c. Setting the gradient threshold to $\langle\Delta I\rangle'(T) = 0.2$ resulted in $T_c(^{13}C) = 313.73\pm1.4$ K and $T_c(^{19}F) = 307.63\pm1.4$ K. In this region a change of the gradient threshold by $\Delta\langle\Delta I\rangle'(T) = \pm0.1$ effects the critical temperature T_c by $\Delta T \approx 1.4$ K. Within the $T_c\pm1.4$ K range, the derived Gibbs' free energy of rotation falls in a narrow range of $\Delta(\Delta G_c^{\ddagger}) \approx 0.08$ kcal/mol.

The rotational barrier of **1** was determined to be $\Delta G_c^{\ddagger}(^{13}C) = 15.11 \pm 0.12$ and $\Delta G_c^{\ddagger}(^{19}F) = 15.65 \pm 0.13$ kcal/mol. The $\Delta G_c^{\ddagger}(^{19}F)$ value is far superior to the $\Delta G_c^{\ddagger}(^{13}C)$ value because ^{19}F NMR spectroscopy offers the advantages of the CF_3 group containing three ^{19}F reporters with 99.99% abundance but only one ^{13}C nucleus with 1.07% natural abundance.

Our best measurement of the rotational barrier of **1** is $\Delta G_c^{\ddagger}(^{19}F) = 15.65 \pm 0.13$ kcal/mol and the rotational barrier $\Delta G_c^{\ddagger}(\mathbf{4}) = 15.9$ kcal/mol was determined computationally for model **4**.[12] This excellent agreement justifies the suitability of **4** as a physically meaningful model of **1**, validates the Boltzmann statistics applied for the determination of the observable rotational barrier resulting from the equilibration of four unique minima via eight rotation-inversion pathways,[12] and that similar minima of **1** equilibrate by traversing similar transition paths.

It was the goal of our study to develop a general method for the derivation of rotational energy barriers from experimental NMR data with the specific aim to test the results of our computational work on the Boltzmann analysis of a two-ensemble system modeling the CN rotational barrier in trifluoroethyl carbamates. The agreement between our experimental and our computational determinations of the rotational barrier is excellent. Any errors associated with the experimental and computational studies are well within tolerable limits.

Acknowledgments

This work was supported by Grant No. 1665487 from the National Science Foundation. We thank Dr. Lingyu Chi and Dr. Klaus Woelk for assistance in the VT NMR measurements of **1**. We thank Dr. Nathan Leigh for useful discussion about sigmoidal line shapes. We appreciate the thoughtful and constructive comments by the Reviewers.

Keywords

Fluorinated Carbamates, *E*/*Z*-Isomerization, Variable Temperature NMR Spectroscopy, Eyring-Polanyi Equation, Lorentzian Line Fitting

Supporting Information

Two tables showing the temperature dependence of the Lorentzian parameters of **1** as a function of temperature for the ^{13}C (Table S1) and ^{19}F (Table S2) data sets.

References

[1] C. Dugave, L. Demange, *Chem. Rev.* **2003**, 103, 2475-2532.

[2] V. Krishnan, S. Vazquez, K. Maitra, S. Maitra, *Chem. Phys. Lett.* **2017**, 689, 148-151.

[3] G. Meng, S. Shi, R. Lalancette, R. Szostak, M. Szotak, *J. Am. Chem. Soc.* **2018**, 140, 727-734.

[4] K. Wiberg, *J. Org. Chem.* **2019**, 84, 10938-10945.

[5] P. Stilbs, S. Forsen, *J. Phys. Chem.* **1971**, 75, 1901-1902.

[6] V. Bryantsev, T. Firman, B. Hay, *J. Phys. Chem. A* **2005**, 109, 832-842.

[7] C. Cox, T. Lectka, *J. Org. Chem.* **1998**, 63, 2426-2427.

[8] M. Deetz, C. Forbes, M. Jonas, J. Malerich, B. Smith, O. Wiest, *J. Org. Chem.* **2002**, 67, 3949-3952.

[9] A. L. Moraczewski, L. A. Banaszynski, A. M. From, C. A. White, B. D. Smith, *J. Org. Chem.* **1998**, 63, 7258-7262.

[10] E. N. Prabhakaran, S. Tumminakatti, K. Vats, S. Ghosh, *RSC Adv.* **2020**, 10, 11871-11875.

[11] B. Jameson, R. Glaser, *ChemistrySelect* **2022**, 7, e202203132 (1-6).

[12] B. Jameson, R. Glaser, *ChemPhysChem* **2023**, 24, e202200442 (1-16).

[13] H. M. McConnell, *J. Chem. Phys.* **1958**, 28, 430-431.

[14] W. E. Stewart, T. H. Siddall, *Chem. Rev.* **1970**, 70, 517-551.

[15] H. Eyring, *J. Chem. Phys.* **1935**, 3, 107-115.

[16] J. Kincaid, H. Eyring, A. Stearn, *Chem. Rev.* **1941**, 28, 301-365.

[17] A. Allerhand, H. S. Gutowsky, J. Jonas, R. A. Meinzer, *J. Am. Chem. Soc.* **1966**, 88, 3185-3194.

[18] J. Sandström, *Dynamic NMR Spectroscopy*, Elsevier Publishers, Waltham MA, **1982**, 96.

[19] A. D. Bain, G. J. Duns, *Can. J. Chem*. **1996**, 74, 819-824.

[20] A. D. Bain, R. A. Bell, D. A. Flecher, P. Hazendonk, R. A. Maharajh, S. Rigby, J. F. Valliant, *J. Chem. Soc., Perkin Trans. 2* **1999**, 1447-1454.

[21] A. Li, X. Luo, D. Chen, L. Li, H. Lin, J. Gao, *Anal. Chem.* **2023**, 95, 70-82.

[22] V. Panakkal, D. Havlicek, E. Pavlova, M. Filipová, S. Bener, D. Jirak, O. Sedlacek, *Biomacromolecules* **2022**, 23, 4814-4824.

[23] K. B. Ekanayake, M. C. Mahawaththa, H. Qianzhu, E. H. Abdelkader, J. George, S. Ullrich, R. B. Murphy, S. E. Fry, J. Johansen-Leete, R. J. Payne, C. Nitsche, T. Huber, G. Otting, *J. Med. Chem.* **2023**, 66, 5289-5304.

[24] J. Blahut, K. Bernášek, A. Gálisová, V. Herynek, I. Císařova, J. Kotek, J. Lang, S. Matějková, P. Hermann, *Inorg. Chem.* **2017**, 56, 13337-13348.

[25] W. Reynolds, D. Wood, *Can. J. Chem.* **1969**, 47, 1295-1309.

[26] A. Muelleman, R. Glaser, *J. Chem. Educ.* **2018**, 95, 476-481.

[27] L. Petrakism, *J. Chem. Educ.* **1967**, 44, 432.

[28] David R. Lide, ed., CRC Handbook of Chemistry and Physics, Internet Version 2005, <http://www.hbcpnetbase.com>, CRC Press, Boca Raton, FL, **2005**.